First-Principles Bottom-Up Study of 1D to 3D Magnetic Transformation in the Copper Pyrazine Dinitrate S=1/2 Antiferromagnetic Crystal

ARTICLE *in* INORGANIC CHEMISTRY · FEBRUARY 2010

Impact Factor: 4.76 · DOI: 10.1021/ic902139h · Source: PubMed

1750 *Inorg. Chem.* **2010**, *49*, 1750–1760
DOI: 10.1021/ic902139h

Inorganic Chemistry
Article

First-Principles Bottom-Up Study of 1D to 3D Magnetic Transformation in the Copper Pyrazine Dinitrate $S = {}^1/_2$ Antiferromagnetic Crystal

J. Jornet-Somoza,[†] M. Deumal,*[,†] M. A. Robb,[‡] C. P. Landee,[§] M. M. Turnbull,[⊥] R. Feyerherm,[¶] and J. J. Novoa*[,†]

[†]*Departament de Química Física and IQTCUB, Facultat de Química, Universitat de Barcelona, Martí i Franquès 1, 08028 Barcelona, Spain,* [‡]*Department of Chemistry, Imperial College London, South Kensington Campus, SW7 2AZ London, U.K.,* [§]*Department of Physics,* [⊥]*Carlson School of Chemistry and Biochemistry, Clark University, 950 Main Street, Worcester, Massachusetts 01610, and* [¶]*Helmholtz-Zentrum Berlin für Materialien und Energie, 14109 Berlin, Germany*

Received October 28, 2009

On the basis of magnetic susceptibility and heat capacity data, copper pyrazine dinitrate crystal [abbreviated $CuPz(NO_3)_2$] has long been considered a good prototype for $S = {}^1/_2$ antiferromagnetic (AFM) Heisenberg chain behavior down to 0.05 K. However, a recent muon-spin rotation experiment indicated the presence of a previously unnoticed 1D to 3D magnetic transition below 0.107 K. Our aim in this work is to perform a rigorous quantitative study of the mechanism of this 1D−3D magnetic transformation, by doing a first-principles *bottom-up* study of the $CuPz(NO_3)_2$ crystal at 158 K, where the magnetic properties are clearly 1D, and at 2 K, at which the neutron structure (reported in this work) is considered nearly identical with that below 0.1 K (due to small thermal effects). A change in the magnetic topology is found between these two structures: at 158 K, there are isolated AFM spin chains ($J_{intra} = -5.23$ cm^{-1}), while at 2 K, the magnetic chains ($J_{intra} = -5.96$ cm^{-1}) weakly interact (the largest of the J_{inter} parameters is -0.09 cm^{-1}). This change is caused by thermal contraction upon cooling (no crystallographic phase transition is detected down to 2 K, and one will not likely occur below that temperature). The computed and experimental magnetic susceptibility $\chi(T)$ curves are nearly identical. The calculated heat capacity $C_p(T)$ curve has a maximum at 6.92 K, close to the 5.20 K maximum found in the experimental curve at zero external field. In spite of the 3D magnetic topology of the crystal at low temperature, the magnetic susceptibility and heat capacity curves behave as a pure 1D AFM chain in all regions because of the large J_{intra}/J_{inter} ratio (66.2 in absolute value) and the effect of including the J_{inter} interactions will not be easily appreciated in any of these experiments. The impact of the presence of odd- and even-membered regular AFM finite chains in the $CuPz(NO_3)_2$ crystal has also been evaluated. Odd-membered interacting chains produce an increase in both $\chi(T)$ and $C_p(T)$ curves when the temperature is very close to zero, in agreement with the experimental observations, while even-membered chains produce a small shoulder in the $C_p(T)$ curve between 0.8 and 5 K. No changes are seen in the remaining regions. Concerning the spin gap, odd-membered chains present a quasi-zero gap but the finite even-membered chains still have a sizable one. Finally, the effect of increasing the magnitude of J_{inter} was investigated by fixing the value of J_{intra} to that found for the 2 K $CuPz(NO_3)_2$ crystal. The magnetic susceptibility and heat capacity curves remain practically unchanged.

Introduction

Progress in molecular magnets over the past several decades has allowed the systematic development of molecule-based ferrimagnets with room temperature spontaneous moments,[1] molecule-based ferromagnets that are simultaneously conducting,[2] organic spin ladders,[3] and other types of magnets. Understanding the magnetic exchange interactions in these systems and the magnetic dimensionality that they generate in any given crystal is essential for the development of new molecule-based magnets with improved properties. The advances in computational quantum chemistry, in conjunction with the revolution of computer technology, have enable ab initio calculations to provide reliable *quantitative* estimates for the magnetic interactions. These unprecedented advances mean that ab initio calculations based only upon knowledge of a crystal structure will be able to play a major role in the engineering of new molecule-based magnets.

*To whom correspondence should be addressed. E-mail: merce.deumal@ub.edu (M.D.); juan.novoa@ub.edu (J.J.N).

(1) Mallah, T.; Theibaut, S.; Verdaguer, M.; Veillet, P. *Science* **1993**, *262*, 1554.
(2) Coronado, E.; Galán-Mascarós, J. R.; Gómez-García, C. J.; Laukhin, V. *Nature* **2000**, *408*, 447.
(3) Arcon, D.; Lappas, A.; Margadonna, S.; Prassides, K.; Ribera, E.; Veciana, J.; Rovira, C.; Henriques, R. T.; Almeida, M. *Phys. Rev. B* **1999**, *60*, 4191.

 Published on Web 01/20/2010

A method capable of rationalizing the magnetism of molecule-based crystals is the recently introduced first-principles *bottom-up* procedure,[4] previously shown to describe properly the experimentally known magnetic properties of a variety of molecule-based magnets showing different magnetic dimensionalities, ranging from 0D to 3D.[5] A first-principles *bottom-up* study of a crystal requires the successive realization of four steps: (1) analysis of the crystal, to find all unique radical−radical pairs, (2) computation of the J_{AB} magnetic exchange interactions for all unique radical−radical pairs, (3) definition of the magnetic topology of the crystal (i.e., the network of magnetic interactions that the non-negligible J_{AB} magnetic interactions create among the radicals of the crystal), and (4) rigorous calculation of the macroscopic magnetic properties (magnetic susceptibility, heat capacity, etc.). Previous theoretical studies on magnetism performed steps 1 and 2 using first-principles calculations but not computing the macroscopic magnetic properties[6] (steps 3 and 4). Alternatively, other theoretical works only compute the magnetic properties (step 4) using assumed values of the magnetic interactions in the Heisenberg Hamiltonian.[7] Our first-principles *bottom-up* procedure brings together these two well-known approaches, using as the connecting tool the minimal magnetic model space (selected in step 3 after computing all J_{AB} and looking at the magnetic topology that they generate in the crystal) and allows one to contrast the computed results obtained in step 4 with the macroscopic experimental magnetic data. Besides reproducing well the experimental magnetic properties of many molecule-based magnets, this procedure agrees with the results of many analytical models whenever the studied system obeys the magnetic topology assumed in the model. In particular, the results reported by the Bonner−Fisher model[8] used for 1D systems are also obtained out of a first-principles *bottom-up* study when the magnetic topology is a chain. Finally, it is worth pointing out that the first-principles *bottom-up* procedure allows the study of any kind of magnetic topology. Thus, it enables one to investigate the effects of a change in the magnetic topology of a crystal, by applying the procedure to a structure determined above and below the temperature where the change in topology takes place.

As a demonstration of these advances, we examine in this work the change in the magnetic dimensionality in copper pyrazine dinitrate,[9−12] henceforth abbreviated as $CuPz(NO_3)_2$. This system was considered as an excellent example of a 1D Heisenberg $S = {}^1/_2$ antiferromagnet down to 0.05 K[9−11] until recent muon-rotation experiments showed the presence of a previously unnoticed 1D−3D magnetic transition below 0.107 K.[12] Ideal 1D Heisenberg antiferromagnetic (AFM) systems are expected to be gapless (zero spin gap) and also should present no long-range magnetic order for $T > 0$ K.[8] Furthermore, they are good candidates for the study of quantum fluctuations (i.e., zero-temperature phase transitions at $|\mathbf{B}| = |2J/g_B|$[13]). Thus, the lack of 1D dimensionality at low T is relevant. Such a change in dimensionality in $CuPz(NO_3)_2$ will be analyzed in this work by comparing the results of a first-principles *bottom-up* study of a structure obtained at 158 K,[11] a region where $CuPz(NO_3)_2$ is known to behave as a 1D regular AFM chain, and a newly determined 2 K neutron diffraction structure (CCDC 761445), which also can be taken as a good representation of $CuPz(NO_3)_2$ around 0.1 K given the small thermal contraction effects expected for the crystal below 2 K.

Computational Details

In this section, we will briefly describe the main steps and underlying physics behind the first-principles *bottom-up* procedure that we apply to the study of the $CuPz(NO_3)_2$ crystal. For the interested reader, a detailed mathematical and physical account of the procedure is available in the literature.[4]

The first-principles *bottom-up* procedure requires the successive realization of the following four steps:

Step 1: Analysis of the crystal structure in order to find all unique A−B radical−radical pairs that might be responsible for the microscopic magnetic interactions. In practical terms, such a selection is done by identifying each symmetry-unique radical A and then choosing all A−B radical pairs, *di*, whose interpair distance is smaller than a given threshold value.

Step 2: Computation of the microscopic J_{AB} magnetic interactions for all A−B radical−radical pairs selected in the previous step. The $CuPz(NO_3)_2$ crystal consists of diamagnetic Pz and NO_3^- ligands coordinated to Cu^{II}, which has an unpaired electron. Therefore, any radical−radical pair can present either a singlet or triplet electronic state. The value of J_{AB} for each pair is then obtained from the energy difference between the open-shell singlet (E_{BS}^S) and triplet (E^T) states, both at the crystal geometry (158 and 2 K). We computed

(4) Deumal, M.; Bearpark, M. J.; Novoa, J. J.; Robb, M. A. *J. Phys. Chem. A* **2002**, *106*, 1299.

(5) (a) Deumal, M.; Bearpark, M. J.; Robb, M. A.; Pontillon, Y.; Novoa, J. J. *Chem.—Eur. J.* **2004**, *10*, 6422. (b) Deumal, M.; Mota, F.; Bearpark, M. J.; Robb, M. A.; Novoa, J. J. *Mol. Phys.* **2006**, *104*, 857. (c) Jornet, J.; Deumal, M.; Ribas-Ariño, J.; Bearpark, M. J.; Robb, M. A.; Hicks, R. G.; Novoa, J. J. *Chem.—Eur. J.* **2006**, *12*, 3995. (d) Shapiro, A.; Landee, C. P.; Turnbull, M. M.; Jornet, J.; Deumal, M.; Novoa, J. J.; Robb, M. A. *J. Am. Chem. Soc.* **2007**, *129*, 952.

(6) (a) Wind, P.; Guihéry, N.; Malrieu, J. P. *Phys. Rev. B* **1999**, *59*, 2556. (b) Moreira, I. P. R.; Illas, F.; Calzado, C. J.; Sanz, J. F.; Malrieu, J. P.; Ben Amor, N.; Maynau, D. *Phys. Rev. B* **1999**, *59*, R6593. (c) Mitani, M.; Mori, H.; Takano, Y.; Yamaki, D.; Yoshioka, Y.; Yamaguchi, K. *J. Chem. Phys.* **2000**, *113*, 4035. (d) Blanchet-Boiteux, C.; Mouesca, J. M. *J. Phys. Chem. A* **2000**, *104*, 2091. (e) Rodriguez-Fortea, A.; Alemany, P.; Alvarez, S.; Ruiz, E. *Chem.—Eur. J.* **2001**, *7*, 627. (f) Illas, F.; Moreira, I. D. R.; de Graaf, C.; Barone, V. *Theor. Chem. Acc.* **2000**, *104*, 265. (g) Kolczewski, C.; Fink, K.; Staemmler, V. *Int. J. Quantum Chem.* **2000**, *76*, 137.

(7) (a) Baker, G. A.; Rushbrooke, G. S.; Gilbert, H. E. *Phys. Rev. A* **1964**, *135*, 1272. (b) Duffy, W.; Barr, K. P. *Phys. Rev.* **1968**, *165*, 647. (c) Diederix, K. M.; Blöte, H. W. J.; Groen, J. P.; Klaassen, T. O.; Poulis, N. J. *Phys. Rev. B* **1979**, *19* 420. (d) Hall, J. W.; Marsh, W. E.; Weller, R. R.; Hatfield, W. E. *Inorg. Chem.* **1981**, *20*, 1033. (e) Hatfield, W. E. *J. Appl. Phys.* **1981**, *52*, 1985. (f) Coronado, E.; Drillon, M.; Fuertes, A.; Beltran, D.; Mosset, A.; Galy, J. *J. Am. Chem. Soc.* **1986**, *108*, 900. (g) Borrás-Almenar, J. J.; Coronado, E.; Curely, J.; Georges, R.; Gianduzzo, J. C. *Inorg. Chem.* **1994**, *33*, 5171. (h) Barnes, T.; Riera, J. *Phys. Rev. B* **1994**, *50*, 6817. (i) Borrás-Almenar, J. J.; Clemente-Juan, J. M.; Coronado, E.; Lloret, F. *Chem. Phys. Lett.* **1997**, *275*, 79. (j) Barnes, T.; Riera, J.; Tennant, D. A. *Phys. Rev. B* **1999**, *59*, 11384. (k) Borrás-Almenar, J. J.; Clemente-Juan, J. M.; Coronado, E.; Tsukerblat, B. S. *Inorg. Chem.* **1999**, *38*, 6081. (l) Borrás-Almenar, J. J.; Clemente-Juan, J. M.; Coronado, E.; Tsukerblat, B. S. *J. Comput. Chem.* **2001**, *22*, 985.

(8) Bonner, J. C.; Fisher, M. E. *Phys. Rev.* **1964**, *135*, A640.

(9) Losee, D. B.; Richardson, H. W.; Hatfield, W. E. *J. Chem. Phys.* **1973**, *59*, 3600.

(10) Mennenga, G.; de Jongh, L. J.; Huiskamp, W. L.; Reedijk, J. *J. Magn. Magn. Mater.* **1984**, *44*, 89.

(11) Hammar, P. R.; Stone, M. B.; Reich, D. H.; Broholm, C.; Gibson, P. J.; Turnbull, M. M.; Landee, C. P.; Oshikawa, M. *Phys. Rev. B* **1999**, *59*, 1008.

(12) Lancaster, T.; Blundell, S. J.; Brooks, M. L.; Baker, P. J.; Pratt, F. L.; Manson, J. L.; Landee, C. P.; Baines, C. *Phys. Rev. B* **2006**, *73*, 020410(R).

(13) Sachdev, S. In *Dynamical Properties of Unconventional Magnetic Systems*; Skjeltorp, A. T., Sherrington, D., Eds.; NATO Advanced Science Institute Series E349; Kluwer: Dordrecht, The Netherlands, 1998.

both energies using the B3LYP functional,[14] the Ahlrichs-pVDZ[15] basis set for Cu, and a 6-31+G(d)[16] basis set for the remaining atoms. For a proper description of the open-shell singlet, the broken-symmetry approximation was used.[17] Within this approximation, the value of J_{AB} is obtained as $2J_{AB} = 2(E_{BS}^{S} - E^{T})$,[18] (the expression for J_{AB} derives from the original broken-symmetry equations[17] when the SOMO orbitals of the two radicals do not overlap). For magnetic superexchange interactions, although its use has been controversial, it provides results closer to the experimental values in most cases.[19] All of the B3LYP calculations on the radical pairs were done using *Gaussian-03*.[20]

Step 3: Definition of the magnetic topology of the crystal and corresponding minimal magnetic model using the non-negligible J_{AB} values. Two neighboring A−B radical sites are connected whenever its magnetic interaction presents a $|J_{AB}|$ value larger than a given threshold. The magnetic topology is then defined in terms of how non-negligible J_{AB} interactions propagate along the crystal axes. Complementarily, the minimal magnetic model is defined as the smallest set of radicals that include all non-negligible J_{AB} interactions in a ratio as close as possible to that found in the infinite crystal. The repetition of such a minimal model along the crystallographic (*a*, *b*, and *c*) directions should regenerate the magnetic topology of the full crystal (a useful test to check the validity of the selected model spaces). The radical centers constituting the minimal magnetic model define a spin space that is used to compute the matrix representation of the corresponding Heisenberg Hamiltonian.[18]

Step 4: The Heisenberg Hamiltonian matrix is diagonalized to obtain the energy for all possible spin states. The size of the corresponding basis set increases with the number of doublet radical centers N of the minimal magnetic model as $N!/[(N/2)!(N/2)!]$. Current computer limitations allow us up to 16 doublet centers. Notice that the only parameters required to compute that matrix representation of the Heisenberg Hamiltonian are the J_{AB} parameters computed in step 2. The obtained energies are then used to compute the magnetic susceptibility $\chi(T)$ and/or heat capacity $C_p(T)$ using the appropriate expressions obtained from a statistical mechanics treatment.

2 K Neutron Study

Neutron diffraction at 2 K was carried out on the BER-II reactor of Helmholtz Zentrum Berlin using the fine-resolution powder diffractometer E9 (Table 1). The neutron wavelength provided by the germanium monochromator was 1.7979 Å. The sample was encapsulated in a vanadium can and cooled in a ^{4}He-flow cryostat. Rietveld analysis of the diffraction data, taken at 2 and 298 K, was carried out using the WinPLOTR/Fullprof package.[21] The diffraction data showed that the sample was a single phase. The refinement indicated a degree of deuteration of 93%. The structural parameters observed at 2 K, relevant for the present study, are listed in a CIF file of the crystal structure, which is given in the Supporting Information and can be downloaded from Cambridge Structural Database (CCDC 761445).

Table 1. Crystallographic Data for the 2 K Neutron Diffraction of $CuPz(NO_3)_2$ Crystals

empirical formula	$C_4H_4N_4O_6Cu$
fw	229.6
radiation	neutron, wavelength 1.7979
cryst syst	orthorhombic
cryst habit	blue powder
space group	*Pmna*
Unit Cell Dimensions	
a, Å	6.69166(6)
b, Å	5.10538(4)
c, Å	11.60022(9)
V, Å^3	396.304(6)
Z	2
size, mm	powder
F(000)	266
Data Collection	
temperature, K	2
max., min transmn	0.7556, 0.3177
reflns collected	304
θ range, deg	−0.927 to +78.90
ranges of *h*, *k*, *l*	$0 \le h \le 7$ $0 \le k \le 5$ $0 \le l \le 11$
Refinement	
data/restraints/param	304/0/32
Rietveldt *R* factors	
R_p	0.123
R_{wp}	0.136
R_{exp}	0.0496

Results and Discussion

In order to rationalize the magnetic properties of $CuPz(NO_3)_2$, we performed two separate first-principles *bottom-up* four-step theoretical studies based on the 158 and 2 K crystal structures [the 2 K structure is taken in this work as a good representation of $CuPz(NO_3)_2$ around 0.1 K given the small thermal contraction effects expected below 2 K]. The 158 K structure, whose main features are depicted in Figure 1, was obtained from X-ray diffraction and was taken from the literature.[11] The 2 K structure was obtained from neutron diffraction experiments as part of this study. The resulting crystal structure observed at 2 K (the CIF file is given in the Supporting Information) is essentially identical with that at ambient temperature. Only slight variations of the lattice parameters and fractional coordinates are found (Table 2 collects the cell parameters for both structures).

(14) (a) Becke, A. D. *Phys. Rev. A* **1988**, *38*, 3098. (b) Lee, C.; Yang, W.; Parr, R. G. *Phys. Rev. B* **1988**, *37*, 785. (c) Becke, A. D. *J. Chem. Phys.* **1993**, *98*, 5648.

(15) Schafer, A.; Horn, H.; Ahlrichs, R. *J. Chem. Phys.* **1992**, *97*, 2751.

(16) (a) Hariharan, P. C.; Pople, J. A. *Theor. Chim. Acta* **1973**, *28*, 213. (b) Francl, M. M.; Pietro, W. J.; Hehre, W. J.; Binkley, J. S.; Gordon, M. S.; DeFrees, D. J.; Pople, J. A. *J. Chem. Phys.* **1982**, *77*, 3654.

(17) (a) Noodlemann, L. *J. Chem. Phys.* **1981**, *74*, 5737. (b) Noodlemann, L. *Chem. Phys.* **1986**, *109*, 131.

(18) We have used the following general form of the Heisenberg Hamiltonian because it is more convenient for our computer codes: $\hat{H} = -2\sum_{A>B} J_{AB}\left(\hat{S}_A\cdot\hat{S}_B + \frac{1}{4}\hat{I}_{AB}\right)$ where A and B indexes run over all non-negligible different radical pairs in the minimal model space, $\hat{I}_{AB}$ is the identity operator, and $\hat{S}_A$ and $\hat{S}_B$ are the spin operators acting on radicals A and B of the A−B radical pair. It is worth pointing out that the energy spectrum computed using this Hamiltonian results in the same energy differences between different eigenvalues as those obtained using the more common expression: $\hat{H} = -2\sum_{A>B} J_{AB}\hat{S}_A\cdot\hat{S}_B$.

(19) For instance, see:(a) Ribas-Ariño, J.; Novoa, J. J.; Miller, J. S. *J. Mater. Chem.* **2006**, *16*, 2600. (b) Ruiz, E.; Alvarez, S.; Cano, J.; Polo, V. *J. Chem. Phys.* **2005**, *123*, 164110. (c) Adamo, C.; Barone, V.; Bencini, A.; Broer, R.; Filatov, M.; Harrison, N. M.; Illas, F.; Malrieu, J. P.; Moreira, I. P. R. *J. Chem. Phys.* **2006**, *124*, 107101.

(20) Frisch, M. J.; et al. *Gaussian-03*, revision C.02; Gaussian, Inc.: Wallingford, CT, 2004.

(21) Roisnel, T.; Rodríguez-Carvajal, J. In *Materials Science Forum, Proceedings of the Seventh European Powder Diffraction Conference (EPDIC 7)*, Barcelona, Spain, 2007; Delhez, R., Mittenmeijer, E. J., Eds.; Trans Tech Publications: Zurich, Switzerland, 2000; pp 118−123.

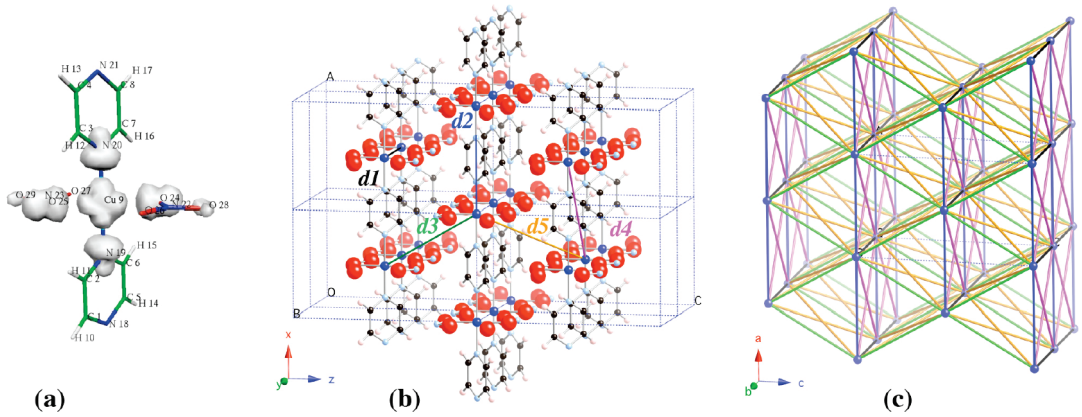

Figure 1. (a) Schematic view of the square-planar coordination of the Cu^{2+} atom (atom numbering is given) and of its spin distribution (the 0.002 au isodensity surface is plotted). (b) Crystal packing of $CuPz(NO_3)_2$ (radical pairs *d1*−*d5* along the *a*, *b*, and *c* axes are indicated). (c) Schematic view of the packing in terms of Cu^{2+} positions, indicating the network of connections generated by all shortest $Cu^{2+}\cdots Cu^{2+}$ contacts (drawn using the same color code as that employed in part b).

Table 2. Cell Parameters (in Å) for the 2 and 158 K Crystals of $CuPz(NO_3)_2$[a]

temperature	*a*	*b*	*c*
2 K	6.69166(6)	5.10538(4)	11.60022(9)
158 K	6.6970(10)	5.1129(10)	11.624(3)
contraction	0.005	0.007	0.024

[a] All cell angles are 90° because both crystals belong to the orthorhombic *Pmna* crystallographic group.

Both crystal structures belong to the orthorhombic *Pmna* crystallographic group with an average change in the crystallographic cell lengths of only 0.012 Å (the maximum is 0.024 Å for the *c* axis, which defines the separation between the planes of $CuPz(NO_3)_2$ chains; see Table2). The shortest intermolecular Cu···Cu, C−H···π (measured as the shortest H···N contact), and O···O contacts in the 158 K crystal are just slightly longer than those in the 2 K crystal: at 158 K, the five unique radical−radical pairs (*d1*−*d5*; Table 3 and Figure 2) have an average value for the shortest Cu···Cu distance of only 0.009 Å longer than that in the 2 K crystal, with an equivalent increase for the H···N(Pz) contact of 0.080 Å and a decrease of 0.003 Å for the O···O contact. At both temperatures, the $CuPz(NO_3)_2$ crystal is characterized by the presence of parallel infinite ···Pz−Cu−Pz−Cu−Pz··· chains along the *a* axis. Nearby chains are linked by attractive C−H···O and C−H···π interactions, whose sum is expected to be stronger than the repulsions between the NO_3^- ligands because, otherwise, a stable crystal would not be formed. The chains pack and form planes along the *ab* axes, which then stack along the *c* axis to form the complete crystal.

The magnetic properties of the $CuPz(NO_3)_2$ crystal result from the interactions among doublet Cu^{2+} ions, each of them tetracoordinated to two diamagnetic neutral pyrazine (Pz) ligands along the *a* axis and two diamagnetic nitrate (NO_3^-) anions along the *bc* plane. The atomic spin population of an isolated $Cu(Pz)_2(NO_3)_2$ aggregate (Figure 1a, obtained from UB3LYP calculations[14] using the Ahlrichs-pVDZ[15] basis set for Cu and a 6-31+G(d)[16] basis set for the remaining atoms) indicates that only 0.58 electrons are located on the Cu^{2+} atom, while 0.10 electrons are located on the two N atoms of the Pz ligand coordinated to Cu and 0.11 electrons on two O atoms of the NO_3^- ligand coordinated to Cu (notice that these values were computed for the 158 K structure but are nearly identical with those obtained for the 2 K structure). Such a spin distribution suggests that both Pz and NO_3^- ligands could play a role in transmitting the magnetic interaction between nearby Cu^{2+} atoms.

Table 3. Values of the J_{AB} Magnetic Exchange Interactions Computed for the *d1*−*d5* Radical Pairs of the $CuPz(NO_3)_2$ Crystal Found in the 158 K X-ray and 2 K Neutron Crystallographic Structures[a]

	Cu···Cu/Å		H···N(Pz)/Å		O···O/Å		$J_{AB}(di)$/cm^{-1}	
dimer *di*	2 K	158 K	2 K	158 K	2 K	158 K	2 K	158 K
d1	5.105	5.112	3.780	3.829	2.736	2.731	+0.06	−0.02
d2	6.692	6.697	4.558	4.538	6.692	6.697	−5.96	−5.23
d3	6.696	6.708	4.733	4.881	3.520	3.509	−0.09	−0.01
d4	8.417	8.425	3.780	3.829	7.229	7.232	+0.03	+0.02
d5	8.420	8.434	5.722	5.894	4.848	4.843	−0.06	0.00

[a] Also indicated are the Cu···Cu, H···N(Pz), and O···O distances for each pair.

The initial experimental magnetic studies[9−11] on $CuPz(NO_3)_2$ concluded that it is almost an ideal 1D magnetic system: although it exhibits a low value for intrachain magnetic exchange constant $J_{intra}(exp) = -3.7$ cm^{-1}, its interchain magnetic exchange constant is 4.4×10^{-3} times smaller,[12] that is, $J_{inter}(exp) = -0.016$ cm^{-1}. Neutron diffraction experiments also confirmed that J_{intra} is the magnetic interaction along the Cu^{2+}−Pz−Cu^{2+} axis.[11] However, recent muon-spin relaxation experiments[12] demonstrated the presence of 3D long-range order below 0.107 K. Note that this long-range order was not detected in previous magnetic susceptibility and specific heat experiments down to 0.070 K.[9−11]

1. Structure and Magnetic Topology of the 158 and 2 K $CuPz(NO_3)_2$ Crystals. As yet mentioned, each radical is a doublet and analysis of the spin density shows that the unpaired electron is mainly localized on the Cu^{2+} atom, although Pz and NO_3^- ligands bear a non-negligible spin contribution. Thus, the A−B pairs were selected by looking at all radical pairs having a Cu···Cu distance smaller than a cutoff of 10.0 Å (this cutoff includes all first-nearest neighbors and the closest second-nearest neighbors). There are only five unique radical−radical pairs, *d1*−*d5* (see Figure 2). The *d1* pair is formed by two radicals of adjacent chains along the *b* axis, with a Cu···Cu distance of 5.112 Å in the 158 K crystal. The *d2* pair is formed by selecting two adjacent

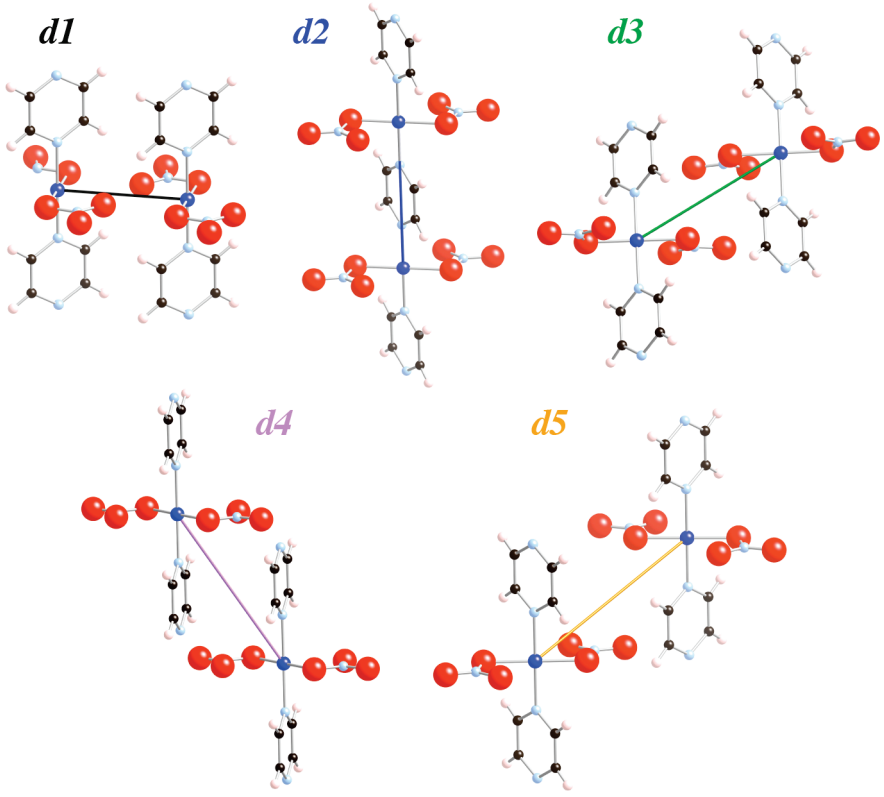

Figure 2. Geometrical disposition of the five unique *di* radical−radical pairs found in the $CuPz(NO_3)_2$ crystal. The *d2* radical pair makes superexchange (or through-bond) magnetic interactions, while all other pairs make direct (or through-space) magnetic interactions.

radicals of the same *a*-axis chain (they are connected by a common Pz molecule), at a Cu···Cu distance of 6.697 Å in the 158 K crystal. The *d3* pair is formed by two radicals of adjacent chains along the *c* axis, with a Cu···Cu distance of 6.708 Å in the 158 K crystal. Finally, *d4* and *d5* pairs are formed by radicals of adjacent chains along the *b* and *c* axes simultaneously, whose Cu···Cu distance is larger than 8.4 Å in both crystals. Notice also that in *d2* the magnetic interaction is through-bond, mediated by the pyrazine ligand (that is, $Cu^{2+}-Pz-Cu^{2+}$), while all other magnetic interactions are through-space of the $Cu^{2+}-NO_3^-\cdots NO_3^--Cu^{2+}$, $Cu^{2+}-Pz\cdots Pz-Cu^{2+}$, and $Cu^{2+}-Pz\cdots NO_3^--Cu^{2+}$ type. These interactions can be properly modeled using the aggregates shown in Figure 2 because all $CuPz(NO_3)_2$ units are neutral and thus no long-range electrostatic Madelung field is required.[22] Figure 1c shows the potential network of magnetic interactions that these five interactions could generate if all were different from zero.

The values for the J_{AB} interactions computed for each nonequivalent radical pair found in the 158 and 2 K crystal structures of $CuPz(NO_3)_2$ are collected in Table 3. In the 158 K crystal, only one interaction is larger than ± 0.05 cm^{-1},[23] $J(d2) = -5.23$ cm^{-1}, which is very close to the experimental value for J_{intra} (-3.7 cm^{-1}). This result is consistent with the experimental observation that superexchange through pyrazine Pz ligands varies between ~0 and about |7| cm^{-1}.[24] The possible impact of cooperative effects in the J_{AB} calculations was evaluated by recomputing the value of $J(d2)$ using a trimer model. Such a trimer was built by selecting three adjacent radicals of the 1D chains. The recomputed $J(d2)$ value is now -5.54 cm^{-1}. Therefore, cooperative effects do not play a relevant role in the magnetic interactions in this system. At this point, one can safely conclude that in $CuPz(NO_3)_2$ the through-bond $Cu^{2+}-Pz-Cu^{2+}$ magnetic interactions, $J(d2)$, are much stronger than the through-space interactions, $J(d1)$ and $J(d3)-J(d5)$, which are of the $Cu^{2+}-NO_3^-\cdots NO_3^--Cu^{2+}$, $Cu^{2+}-Pz\cdots Pz-Cu^{2+}$, and $Cu^{2+}-Pz\cdots NO_3^--Cu^{2+}$ types. Notice also that $Cu^{2+}-NO_3^-\cdots NO_3^--Cu^{2+}$ magnetic interactions found in $CuPz(NO_3)_2$ are much weaker than some $Cu^{2+}-Cl^-\cdots Cl^--Cu^{2+}$ or $Cu^{2+}-Br^-\cdots Br^--Cu^{2+}$ magnetic interactions observed in analogous solids.[25] This fact may suggest that monatomic ligands are more

(22) Kittel, C. *Introduction to Solid State Physics*, 7th ed.; John Wiley & Sons, Inc.: New York, 1996.

(23) DFT accuracy in energies is 10^{-8} au. Thus, we take ± 0.05 cm^{-1} as a threshold value below which J_{AB} are supposed to be negligible. The validity of such a statement in $CuPz(NO_3)_2$ was checked by comparing the results of the macroscopic properties computed when including $J(d1)$ and J(d3) with those obtained when only J(d2) was employed, and they were indistinguishable, as discussed in the main text.

(24) (a) Richardson, H. W.; Wasson, J. R.; Hatfield, W. E. *Inorg. Chem.* **1977**, *16*, 484. (b) Hong, D. M.; Wei, H. H.; Chang, K. H.; Lee, G. H.; Wang, Y. *Polyhedron* **1998**, *17*, 3565. (c) Haynes, J. S.; Sams, J. R.; Thompson, R. C. *Can. J. Chem.* **1988**, *66*, 2079. (d) Haynes, J. S.; Rettig, S. J.; Sams, J. R.; Thompson, R. C.; Trotter, J. *Can. J. Chem.* **1987**, *65*, 420. (e) Belaiche, M.; Benhammou, M.; Drillon, M.; Derory, A.; Soufiaoui, M. *Chem. Phys. Lett.* **2004**, *395*, 75. (f) Awwadi, F. F.; Landee, C. P.; Turnbull, M. M.; Twamley, B.; Wells, B. M. *Polyhedron* **2005**, *24*, 2153.

(25) For Cu(2,5-dimethylpyrazine)Cl_2, magnetic data are fitted to $2J_{intra} = -20$ K $= -13.9$ cm^{-1}, and $2J'_{inter} = -4$ K $= -2.8$ cm^{-1} with $J'/J = 0.20$. See: Awwadi, F. F.; Landee, C. P.; Turnbull, M. M.; Twamley, B.; Wells, B. M. *Polyhedron* **2005**, *24*, 2153For Cu(2,5-dimethylpyrazine)Br_2, larger values of J exchange interaction are found. Turnbull, M. M. Private communication. Notice that, because $Cu^{2+}-Cl^-\cdots Cl^--Cu^{2+}$ and $Cu^{2+}-Br^-\cdots Br^--Cu^{2+}$ magnetic interactions depend on the distance and orientation of the interacting fragments, some of them are strong and others can be very weak.

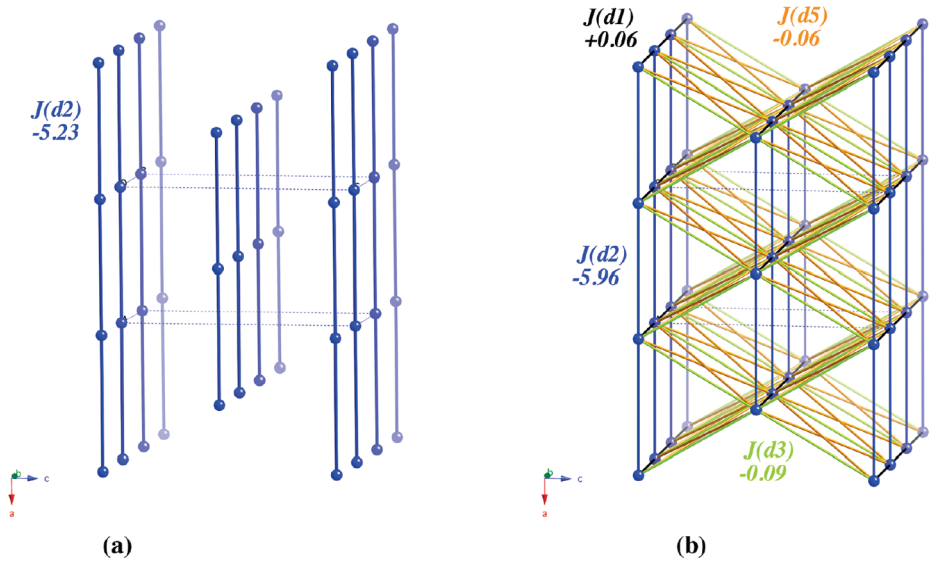

Figure 3. Magnetic topology of the $CuPz(NO_3)_2$ crystal at (a) 158 and (b) 2 K. Only the non-negligible magnetic interactions (J_{AB} values larger than |0.05| cm^{-1}) define the magnetic topology (their values are also given, in cm^{-1}).

effective in mediating through-space magnetic interactions. Further studies on this subject are currently underway.

The previous results indicate that anisotropic thermal contraction of the $CuPz(NO_3)_2$ crystal when cooling from 158 to 2 K induces an increase in the magnitude of the $J(d1-d5)$ parameters: $J(d2)$ is still the strongest magnetic interaction, preserving its AFM character, but now $J(d1)$, $J(d3)$, and $J(d5)$ are larger than ± 0.05 cm^{-1}. As a consequence, the magnetic topology of $CuPz(NO_3)_2$ at 158 K (Figure 3a) consists of isolated 1D chains, in good agreement with the experimental facts. Contrarily, at 2 K the magnetic topology presents a non-negligible 3D character that could affect the magnetic properties at very low temperature (Figure 3b).

2. Calculation of the Magnetic Susceptibility, Heat Capacity, and Spin Gap for the 158 and 2 K $CuPz(NO_3)_2$ Crystal Structures. The energy spectrum was obtained by diagonalizing the matrix representation of the Heisenberg Hamiltonian within an appropriate magnetic model space, as described above. Previous studies on 1D chains[5c] have demonstrated that the macroscopic magnetic properties of an isolated chain can be described by finite chains of n sites (ns model spaces; Figure S1 in the Supporting Information) and that the simulated magnetic susceptibility $\chi(T)$ data agree better with the experimental $\chi(T)$ values as the size of such a ns finite model is increased. Such convergence is also observed to be valid on the 158 K structure of $CuPz(NO_3)_2$ for finite magnetic model spaces that include from 4 up to 12 spin centers (see Figure 4a). Notice that for models larger than 10s the $\chi(T)$ results practically overlap and thus are not shown in Figure 4a. Such a convergence can also be seen in the $\chi T(T)$ curves (see Figure S2 in the Supporting Information). All model spaces reproduce the main features of the experimental curve. However, there is a small difference between the maximum of $\chi(T)$ using a 10s magnetic model and the experimental data, which can be attributed partially to the fact that the experimental data were obtained from powder samples while the computed results only account for single crystals aligned along the z axis [note that $\chi(T)$ values from powder samples are always an upper bound for $\chi_{||}(T)$ from single crystals[9]]. There are also possible minor errors introduced in the computed J_{AB} values by the use of approximate density functional theory (DFT) and truncated basis sets. Finally, it should also be noted that our computed data using the 10s model do not reproduce the strong increase reported in the experimental magnetic susceptibility curve below 0.5 K, which was attributed by the authors to the presence of a mixture of finite chains with odd and even numbers of sites.[10] The impact of these finite fragments on the magnetic susceptibility curve will be addressed further below.

The balanced description of all of the microscopic J_{AB} interactions found in an infinite $CuPz(NO_3)_2$ crystal requires a 3D magnetic building block that includes four adjacent chains with two sites (2s) per chain, a magnetic model hereafter identified as the $4 \times 2s$ model (the name originates from the four chains it contains, each made of two sites; Figure S1 in the Supporting Information). We tested the convergence of the magnetic susceptibility with an increase in the size of the chains by doing calculations with the $4 \times 2s$ and $4 \times 4s$ magnetic models (Figure S1 in the Supporting Information). A good agreement between computed $\chi(T)$ curves was found (Figure 4b).

Looking at the $\chi(T)$ curves computed using 1D and 3D models, it is possible to evaluate quantitatively the impact of including the interchain magnetic interactions in the computation. Figure 4c plots the $\chi(T)$ curves computed using a $4 \times 4s$ 3D model with a parent model where no interchain interactions have been included (the 4s 1D model, for which two different computations were done, depending on $J(d2) = -5.96$ cm^{-1} at 2 K or -5.23 cm^{-1} at 158 K). It is shown that the $\chi(T)$ curve using the $4 \times 4s$ model is practically identical with the $\chi(T)$ curve using the 4s model if computed with the same $J(d2)$ parameter (-5.96 cm^{-1}). Notice that the same 4s 1D model with a $J(d2)$ parameter of -5.23 cm^{-1} shows a slight difference in the $\chi(T)$ curve in the maximum region. In conclusion, the interchain $J(di)$ interactions make an almost negligible impact on the computed $\chi(T)$ curve. In another words,

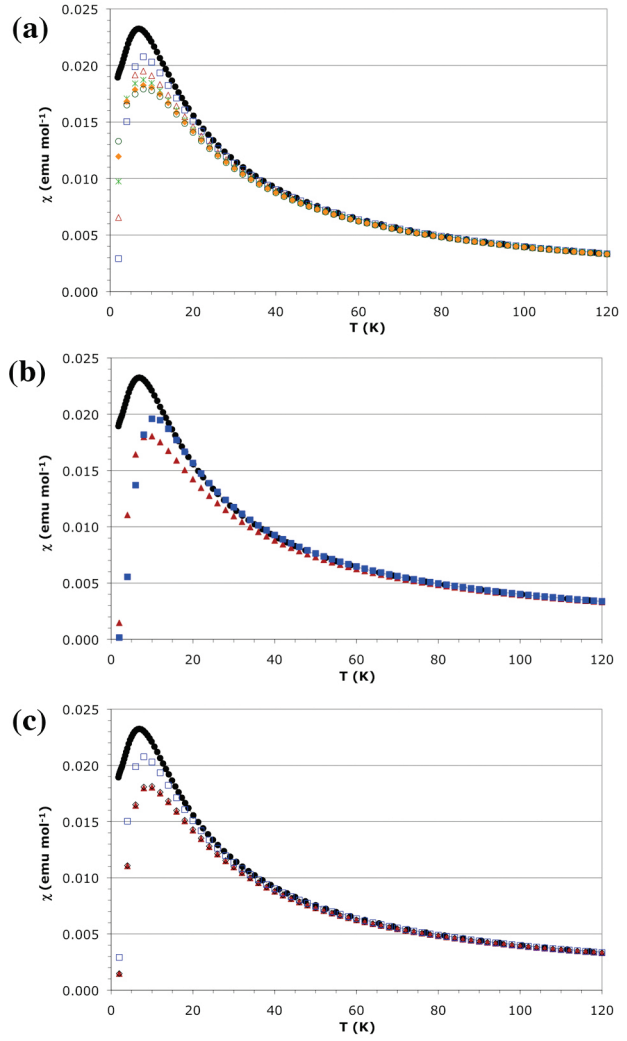

Figure 4. (a) Computed $\chi(T)$ curve for the $CuPz(NO_3)_2$ crystal using the following 1D magnetic model spaces: 4s (blue □), 6s (purple △), 8s (green ×), 10s (orange ◆), and 12s (○). (b) Computed $\chi(T)$ curve for the $CuPz(NO_3)_2$ crystal using 4 × 2s (blue ■) and 4 × 4s (red ▲) 3D magnetic model spaces. (c) Comparison between the $\chi(T)$ curve computed with the 4 × 4s 3D model (red ▲) and the 4s model when $J(d2) = -5.23$ cm^{-1} (blue □) and $J(d2) = -5.96$ cm^{-1} (◇). In all cases, the experimental curve (●) obtained from powder samples is also shown.

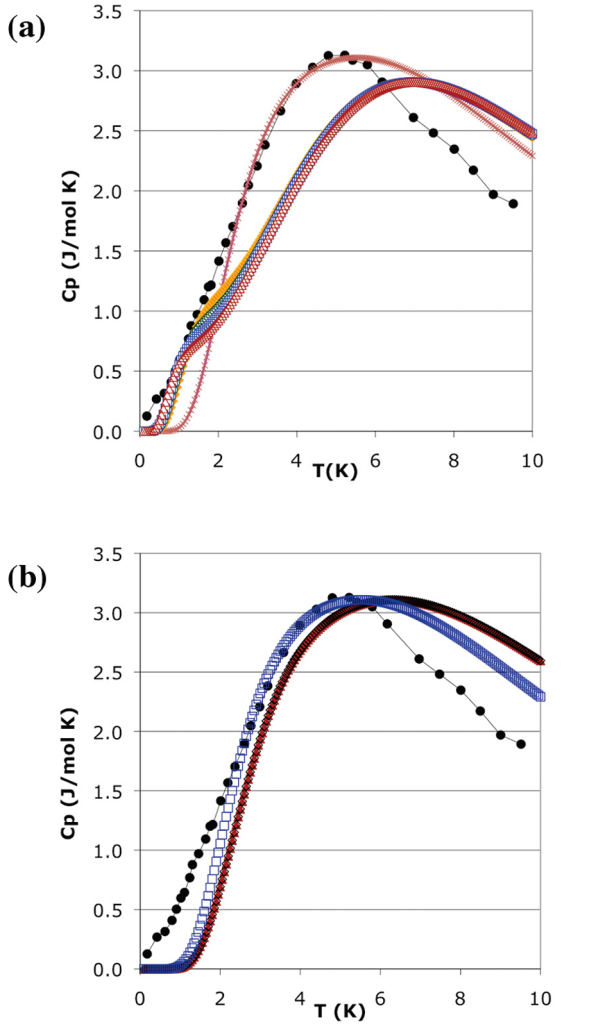

Figure 5. (a) Computed heat capacity, $C_p(T)$, curve for the $CuPz(NO_3)_2$ crystal studied with crystallographic data determined at 158 K using the 4s (red +), 10s (orange ◆), 12s (○), 14s (blue □), and 16s (purple △) 1D magnetic model spaces. (b) Heat capacity curve computed using the 4 × 4s 3D magnetic model space (red ▲), the 1D isolated 4s chain when $J(d2) = -5.96$ cm^{-1} (red +; it is not seen because it overlaps the red triangles), and the same model space when $J(d2) = -5.23$ cm^{-1} (blue □). In all cases, the experimental curve (●) is also shown.

the 1D to 3D change in dimensionality in this crystal cannot be visualized by magnetic susceptibility studies.

The heat capacity curve was also investigated, looking at the change produced when the interchain $J(di)$ interactions were included. Figure 5a shows the heat capacity curves computed using 1D models ranging from 4 to 16 radical sites. With all models, a maximum was found in the heat capacity curve of around 6.92 K, very close to the 5.20 K maximum found in the experimental curve at zero external field[11] and associated with the presence of AFM order. However, it is worth pointing out here that recent studies[26] suggest that the presence of a maximum in the heat capacity curves cannot always be taken as a signature of long-range magnetic order: the absence of a sharp λ peak on that maximum suggests that we are dealing with a Schottky anomaly caused by short-range correlations among the chains. Notice that our computations cannot distinguish between long- and short-range order because of the finite size of our models. It is also worth pointing out that all computed $C_p(T)$ curves using finite-size models ($N > 8$s) present a small shoulder in the 1−2 K region, in agreement with previous results obtained by Bonner and Fisher.[8] The height and temperature of this shoulder decrease as the size of the magnetic chain model is increased (note that the same effect is observed in linear as well as ring models; see Figure S3 in the Supporting Information). The presence of such a shoulder appears during exploration of the low-temperature region in the experimentally measured heat capacity data ($T < 2$ K).[10,11]

The effect on the heat capacity curve of the inclusion of the J_{inter} interactions was studied (see Figure 5b) by comparing the curves computed using a 3D model that includes these interactions (the 4 × 4s 3D magnetic model space) and the corresponding 1D model (1D 4s model, with $J(d2)$ being -5.96 cm^{-1} at 2 K and -5.23 cm^{-1} at 158 K). The 4 × 4s 3D and 4s 1D curves

(26) Sengupta, P.; Sandvik, A. W.; Singh, R. R. P. *Phys. Rev. B* **2003**, *68*, 094423.

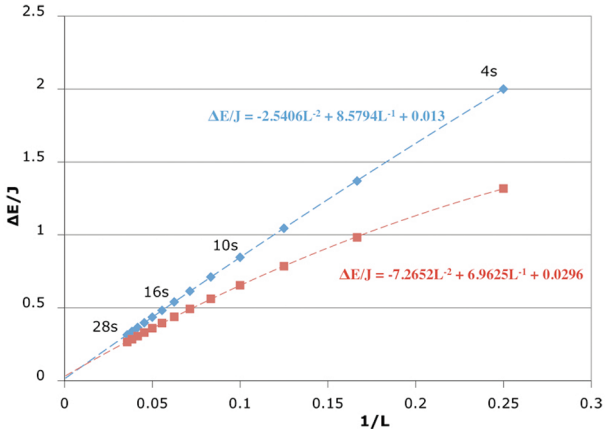

Figure 6. Dependence of the spin gap (ΔE) over J as a function of $1/L$ (L being the length of the spin chain in the finite model employed) for ns models ranging from 4s ($L^{-1} = 0.25$) to 28s ($L^{-1} = 0.036$). Cyclic chains are indicated by blue ◆, while linear chains are identified by red ■.

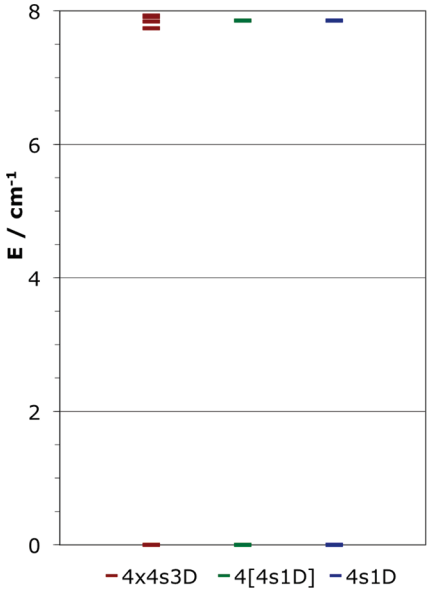

Figure 7. Energy of the lowest-energy states (in cm^{-1}) computed with the four interacting 4s chains (4×4s3D) magnetic model space, an isolated 4s 1D space, and four noninteracting 4s chains (4s[4s1D]) model. In all cases, $J(d2) = -5.96\ cm^{-1}$. In each model, the energy has been measured relative to the ground-state energy.

are almost identical. Therefore, the interchain $J(di)$ interactions make an almost negligible impact on the heat capacity curve. Consequently, the 1D to 3D change in dimensionality in this crystal cannot be visualized by heat capacity studies.

We will finally study the impact of the change of dimensionality on one last macroscopic property: the singlet−triplet spin gap. Although for a perfect 1D magnetic system the singlet−triplet spin gap should be equal to zero,[27] Bonner and Fisher[8] reported a nonzero spin gap due to the finite size effects in the model. In good agreement with Bonner and Fisher, our computations (Figure S4 in the Supporting Information) do not predict zero spin gaps between the ground-state singlet and the lowest-energy excited state (a triplet in the $CuPz(NO_3)_2$ crystal).[28] As is also pointed by Bonner and Fisher, the computed spin gap decreases as the length of the finite magnetic model space is increased. This convergence behavior of the spin gap (ΔE) is usually illustrated by plotting the variation of ΔE as a function of $1/L$, with L being the total length of the finite regular chain in the magnetic model space. In the $CuPz(NO_3)_2$ crystal, the ΔE versus $1/L$ variation is shown in Figure 6 for open and cyclic chains. By fitting the ΔE versus $1/L$ variation to the equation $\Delta E/J = aL^{-2} + bL^{-1} + c$, one can extrapolate the spin gap for an infinite chain: for linear chains, $c = 0.0296$, while for cyclic chains, $c = 0.013$. In both cases, the spin gap ΔE is different from zero (0.176 and 0.077 cm^{-1}, respectively). This fact can be taken as indicative of an error in the estimation or that longer chain models should be used as magnetic models in order to obtain a proper estimate. It is also worth noting that the values of the spin gap computed with and without inclusion of J_{inter} are very similar. This can be shown by comparing the spin gap of an isolated 4s chain (4s 1D model), four noninteracting 4s chains (4[4s 1D] model), and four interacting 4s chains (4 × 4s 3D model) (see Figure 7). The ground state for these three models is always nondegenerate (in Figure 7, the ground states are taken as the origin on the x axis), that is, presents a nonzero spin gap. In all three models, the first excited state is a triplet. The energy of this triplet in the 4[4s 1D] model is tetradegenerate and equal to that for the 4s 1D model. Contrarily, in the 4 × 4s 3D model, the energy of the triplet state is split, but the value of this splitting is very small compared to the spin gap. This splitting originates from the J_{inter} interactions. However, in $CuPz(NO_3)_2$, the J interactions are very small, and their effect on the spin gap is unnoticeable.

In summary, the impact of including the J_{inter} interactions on the computation of the magnetic susceptibility curve, heat capacity curve, and spin gap of the $CuPz(NO_3)_2$ crystal is so small that it will not be easily appreciated in any of these experiments. Because of the large J_{intra}/J_{inter} ratio (66.2 in absolute value when using the largest of the J_{inter} parameters $-0.09\ cm^{-1}$), the magnetic susceptibility and heat capacity curves behave as a pure 1D AFM chain in all regions, although the magnetic topology of the crystal at low temperature is that of a 3D system, as observed by techniques sensitive to that topology (e.g., muon-spin rotation). Therefore, theoretical first-principles *bottom-up* studies provide a proper analysis of the origin and known features of the 1D−3D magnetic transition found in the $CuPz(NO_3)_2$ crystal. The only experimental feature still remaining to be accounted for is the impact of introducing the presence of finite chains in these calculations. They were suggested in the literature to exist on qualitative grounds,[8,10]

(27) (a) Frischmuth, B.; Ammon, B.; Troyer, M. *Phys. Rev. B* **1996**, *54*, R3714. (b) Greven, M.; Birgeneau, R. J.; Wiese, U.-J. *Phys. Rev. Lett.* **1996**, *77*, 1865. (c) Barnes, T.; Dagotto, E.; Riera, J.; Swanson, E. S. *Phys. Rev. B* **1993**, *47*, 3196. (d) Dagotto, E.; Riera, J.; Scalapino, D. *Phys. Rev. B* **1992**, *45*, 5744. (e) White, S. R.; Noack, R. M.; Scalapino, D. J. *Phys. Rev. Lett.* **1994**, *73*, 886. (f) Troyer, M.; Tsunetsugu, H.; Würtz, D. *Phys. Rev. B* **1994**, *50*, 13515. (g) Barnes, T.; Riera, J. *Phys. Rev. B* **1994**, *50*, 6817. (h) Dagotto, E. D.; Rice, T. M. *Science* **1996**, *271*, 618.

(28) The energy spectra obey the following general trends: (a) The relative stability between the lowest-energy states of a given multiplicity increases as S is increased; that is, $E_{LS}(S=0) < E_{LS}(S=1) < ....$ (b) Some of the lowest-energy states of any given multiplicity are discrete and do not form part of the energy band formed by most of the remaining states. (c) The formation of bands (states separated by energy gaps smaller than the thermal energy) is observed when large enough chains are used in the computations.

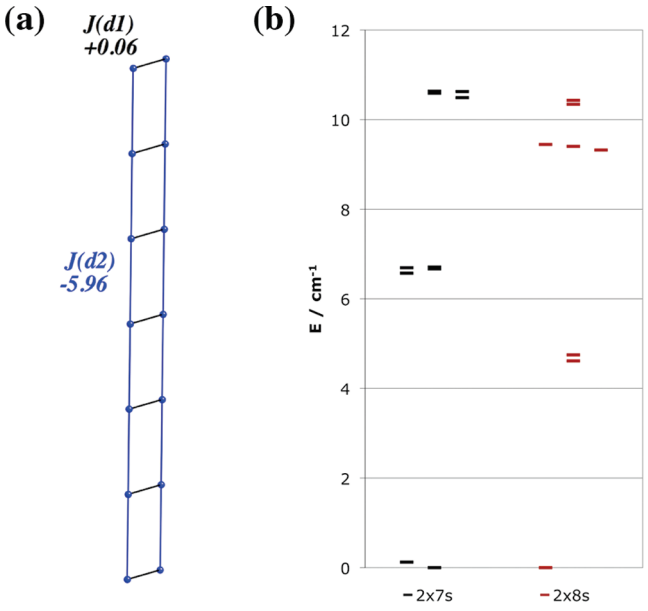

Figure 8. (a) Magnetic topology employed to compute the interaction between two 7s spin chains arranged parallel to each other (2 × 7s model). (b) Energy of the lowest-energy states (in cm^{-1}) computed for the 2 × 7s and 2 × 8s models (for each model, the states of multiplicity $S = 0$, 1, and 2 are represented, ordered from left to right). Note that in the 2 × 7s model the triplet state is the ground state by 0.12 cm^{-1}, while in the 2 × 8s model, the singlet state is the ground state by 4.61 cm^{-1}.

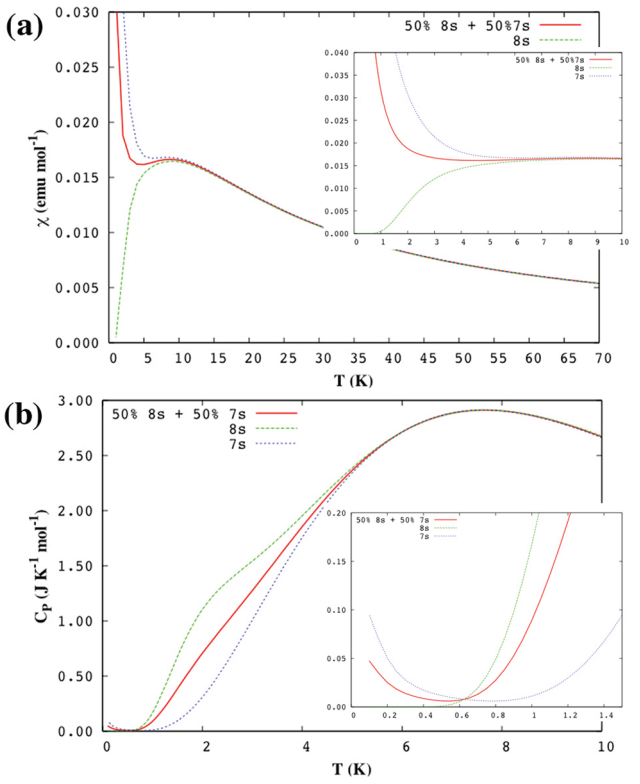

Figure 9. (a) Magnetic susceptibility curves and (b) heat capacity curves computed for the 2 × 7s (in blue) and 2 × 8s (in green) models (the inset shows an expanded view of the heat capacity curve at low temperature). The total curve resulting from the addition of the 2 × 7s and 2 × 8s curves in a 50%/50% ratio is also shown (in red).

although no previous quantitative work has ever studied their effect on the magnetic susceptibility and heat capacity curves of the $CuPz(NO_3)_2$ crystal.

3. Impact of the Presence of Finite Chains on the Macroscopic Magnetic Properties. As mentioned before, the magnetic susceptibility and heat capacity curves observed at very low temperatures ($T < 1$ K) show some effects that have been qualitatively explained by assuming the presence of odd- and even-membered finite chains.[10,29] Notice that, up to now, all simulations have been done using even-membered finite chains. In this section, using the first-principles *bottom-up* results, we will address how the coexistence of odd- and even-membered finite AFM chains affects the previously computed results.

Ideal 1D molecule-based magnets consist of infinite noninteracting spin chains arranged parallel to each other. However, *real* 1D molecule-based magnets present a small number of defects that truncate the ideal infinite spin chains in either odd- or even-membered finite chains. In the $CuPz(NO_3)_2$ crystal, the ground state of an even-membered finite chain with AFM J_{intra} is an open-shell singlet (i.e., each spin-carrying unit of the chain has a spin pointing in the opposite direction than its two adjacent units). Accordingly, for an odd-membered finite chain, the ground state is a doublet. The macroscopic properties of either collinear or parallel even-membered units have been treated before (see Figure 4). Therefore, we only have to address the magnetic properties of odd-membered units from now on. Because the geometry of the defect is not known, we will use a qualitative model in order to understand their interaction.

The study of two interacting odd-membered units arranged parallel was done by selecting two 7s chains, as shown in Figure 8a (hereafter called the 2 × 7s model; among many possibilities, this one was selected because the interchain interactions were the largest ones that also showed an opposite nature to the intrachain interactions). Figure 8b compares the lowest-energy states for the 2 × 7s model with those for the 2 × 8s level, with the latter taken as a prototype of a finite even-membered chain of length similar to that of the 7s chain. The distribution of the energy levels in the 2 × 8s model is similar to that already described for *n*s (*n* = even) models (see Figure S4 in the Supporting Information): there is a ground-state singlet followed by a triplet state. However, in the 2 × 7s model, the lowest-energy singlet state is nearly degenerate to the triplet state, which is slightly more stable because the interaction J_{inter} between the two odd-membered finite AFM chains is ferromagnetic. As shown in Figure 9, such quasi-degeneration has an important impact in the macroscopic magnetic properties because now the triply degenerate triplet state contributes to the magnetic moment even at 0 K. While the magnetic susceptibility curve for the 2 × 8s chain model goes to zero at $T = 0$ K (as corresponds to a singlet ground state), for the 2 × 7s chain model $\chi(T)$ increases as T approaches zero because of a triplet ground state (Figure 9a). As a consequence, the coexistence of odd-membered (7s) and even-membered (8s) chains in the crystal results in the total magnetic susceptibility curve increasing as the temperature goes to zero (see Figure 9a). Notice that the ratio of 50% odd-membered versus 50% even-membered chains has been *statistically* chosen in order to exemplify the coexistence of both finite-membered chains and the global effect on

(29) de Jongh, L. J.; Miedema, A. R. *Adv. Phys.* **1974**, *23*, 1.

the macroscopic properties (see Figure S5 in the Supporting Information for different odd/even ratio distributions). Therefore, we have quantitatively demonstrated that the increase in the magnetic susceptibility curve at very low temperature (<2 K) is due to the presence of magnetically interacting odd- and even-membered finite chains within the crystal.

At this point, it is also worth looking at the effect of these finite chains on the heat capacity $C_p(T)$ curves and the spin gap. As shown in Figure 9b, the presence of finite chains generates two effects in the heat capacity curves: (a) magnetically interacting odd-membered chains (represented by two 7s chains arranged in parallel) produce an increase in the $C_p(T)$ curve when the temperature is very close to zero, and (b) magnetically interacting even-membered chains (two interacting 8s chains arranged in parallel) produce a shoulder in the $C_p(T)$ curve between 0.8 and 5 K (note that this shoulder is also observed using isolated chain models). When even- and odd-membered finite AFM chains coexist, the two effects are generated. At this point, it is important to highlight that the increase in $C_p(T)$ phenomena only appears if there is a small spin gap between the ground state and the first excited state; i.e., J_{inter} is different from zero (see Figure 8b) because otherwise for purely isolated odd-membered chains the ground-state degeneracy cannot produce this effect. The presence of this shoulder, also seen in the experimental curve (Figure 5), went unnoticed up to now and is a direct consequence of the existence of even-membered finite AFM chains within the crystal.

Finally, the effect of having finite chains on the spin gap is depicted in Figure 8b for odd- and even-membered finite AFM chains: in the $CuPz(NO_3)_2$ crystal, odd-membered chains always have a negligible singlet−triplet gap for the two lowest states of this multiplicity (0.12 cm^{-1} for the 2×7s model), while for even-membered finite chains, the spin gap is nonzero (4.61 cm^{-1} for the 2×8s model). Therefore, whenever odd-membered finite chains are present, the net spin gap will be zero.

In summary, the presence of even- and odd-membered finite regular AFM chains induces changes in the macroscopic properties and allows one to explain all regions of the magnetic susceptibility and heat capacity curves of the $CuPz(NO_3)_2$ crystal: magnetically interacting odd-membered chains produce an increase in both $\chi(T)$ and $C_p(T)$ curves when the temperature is very close to zero, and even-membered chains produce a shoulder in the curve between 0.8 and 5 K. No changes are seen in the remaining regions. Concerning the spin gap, odd-membered chains present a negligible gap but finite even-membered chains still have a sizable one.

4. Impact of the Variation of the J_{intra}/J_{inter} Ratio on the 1D to 3D Transition. The large J_{intra}/J_{inter} ratio in the $CuPz(NO_3)_2$ crystal (66.2 in absolute value when using the largest $J_{inter} = -0.09$ cm^{-1}) is the reason why in this crystal the magnetic susceptibility and heat capacity curves can be computed using a pure 1D regular AFM chain model in all regions, although at low temperature the crystal has 3D magnetic topology, as techniques sensitive to that topology observe (e.g., muon-spin rotation). The first-principles *bottom-up* calculations performed in this work indicate that such behavior is caused by the large separation between the singlet ground state and the first triplet excited state compared to the thermal

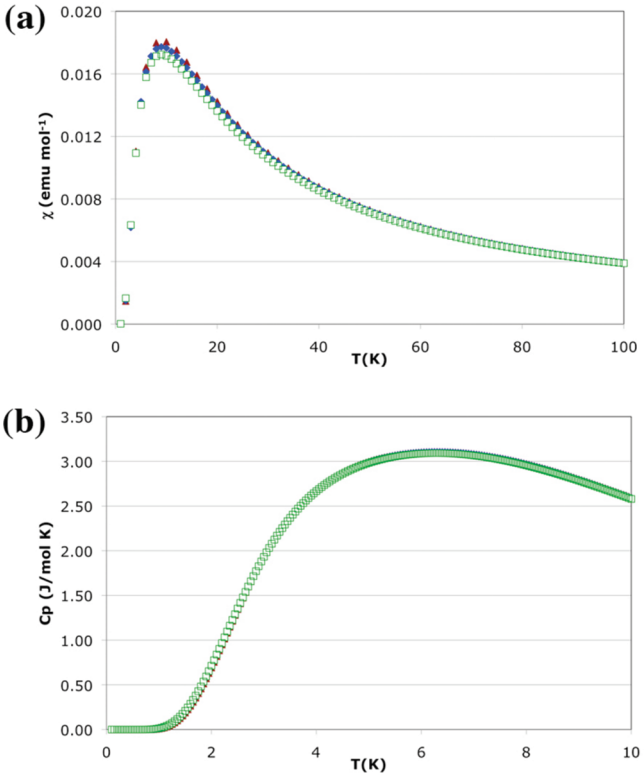

Figure 10. (a) Magnetic susceptibility and (b) heat capacity curves for a hypothetical $CuPz(NO_3)_2$ crystal using the 4×4s 3D model in which all J_{inter} parameters are increased 5 (blue ◆) and 10 times (green □). In both cases, J_{intra} is kept equal to -5.96 cm^{-1}. The curve obtained using the magnetic model with the computed J_{inter} is also represented for comparison (purple ▲).

energy at the region of temperatures where the 1D−3D magnetic transition occurs. However, as shown in Figure 7, such an energy difference can be changed by increasing the splitting of the triplet states, which is determined by the value of J_{inter}. Therefore, as the final step in our study of the 1D to 3D transition in low-dimensional materials, we simulated the behavior of the magnetic susceptibility and heat capacity curves for a hypothetical $CuPz(NO_3)_2$ crystal in which all J_{inter} parameters would be increased by a multiplying factor. The changes in the macroscopic properties will be rationalized by looking at the changes in the energy spectra of the spin states of the crystal (which are the magnetic states in the magnetic model space).

Two initial cases were studied: (1) the J_{intra}/J_{inter} ratio is 5 times smaller, 13.24 obtained by multiplying all J_{inter} by 5 without changing their sign, and (2) the J_{intra}/J_{inter} ratio is 10 times smaller, 6.62, once again obtained by multiplying all J_{inter} by 10 without changing their sign (note that we have preserved the 1D character of the magnetic topology). Other variations such as changing the sign of J_{inter} in various ways are possible, but they were not included in this initial study. The magnetic susceptibility and heat capacity curves of these two cases are shown in Figure 10, while the energies of the lowest-energy states are shown in Figure 11.

The results in Figure 10 indicate that as the J_{intra}/J_{inter} ratio is changed from 66.2 to 13.24 and 6.62 the magnetic susceptibility and heat capacity curves remain practically unchanged. This can be explained by looking at Figure 11

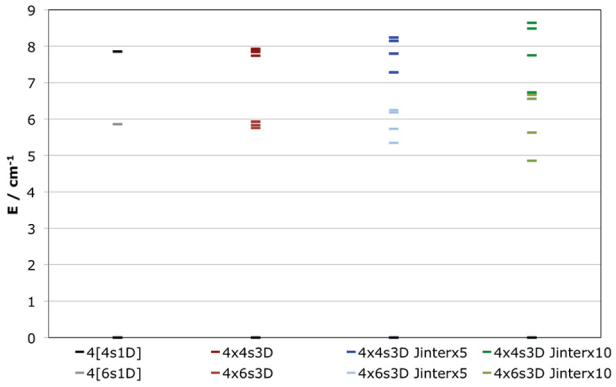

Figure 11. Energy spectra with respect to the ground state for the lowest-energy states computed using the 4 × 4s 3D (up) and 4 × 6s 3D (down) models for a hypothetical $CuPz(NO_3)_2$ crystal in which all J_{inter} parameters are increased 5 and 10 times. The energy spectra for 4[4s 1D] (up) and 4[6s 1D] (down) models (i.e., with no J_{inter}) and for 4 × 4s 3D (up) and 4 × 6s 3D (down) models with the computed J_{inter} are also represented for comparison. In all of these cases, J_{intra} is kept equal to -5.96 cm^{-1} (which is the J_{intra} value at 2 K).

for 4s and 6s magnetic models: although the singlet−triplet gap becomes smaller as J_{intra}/J_{inter} decreases, the variation is small compared to the size of the gap (e.g., when J_{inter} is multiplied by 10, the gap, whose value is 7 cm^{-1}, decreases by 1 cm^{-1}).

Conclusions

Using a first-principles *bottom-up* procedure, we have computed the nature of the J_{AB} magnetic interactions and, from them, the macroscopic properties of the $CuPz(NO_3)_2$ magnet using its 158 and 2 K crystal structures. This system is a prototype of 1D isolated AFM chains that recently has been demonstrated to undergo a transition to 3D long-range order at 0.107 K.[12] Our calculations, using the crystal structure determined at 158 K, indicate that there is a dominant intrachain magnetic interaction, $J_{intra} = -5.23$ cm^{-1}, and three interchain magnetic interactions, $J_{inter} = -0.02, +0.02,$ and -0.01 cm^{-1}, which are numerically negligible for simulation purposes. At 2 K, these values are enhanced ($J_{intra} = -5.96$ cm^{-1} and $J_{inter} = -0.06, -0.09, +0.03,$ and 0.06 cm^{-1}) and the magnetic topology becomes 3D. These values agree well with the experimental estimates[12] ($J_{intra} = -3.7$ cm^{-1} and $J_{inter} = -0.016$ cm^{-1}). The J_{inter} values related to $Cu^{2+}-NO_3^-\cdots NO_3^--Cu^{2+}$ magnetic interactions found in $CuPz(NO_3)_2$ are much weaker than some $Cu^{2+}-Cl^-\cdots Cl^--Cu^{2+}$ or $Cu^{2+}-Br^-\cdots Br^--Cu^{2+}$ magnetic interactions found in analogous solids.[25]

Using the computed J_{intra} and J_{inter} magnetic interactions, we calculated both magnetic susceptibility and heat capacity curves that reproduce the experimental data. The heat capacity curve presents a maximum at 6.92 K, very close to the 5.20 K maximum found in the experimental curve at zero external field. An analysis of the shape of the heat capacity maximum suggested that it is a Schottky anomaly, which cannot be associated with the presence of long-range order. These macroscopic properties are not affected by the inclusion of the very small J_{inter} due to the large J_{intra}/J_{inter} ratio; that is, the macroscopic magnetic properties are well described by a pure 1D AFM model (regular chain). This fact explains why this model can be used to fit experimental data obtained at high enough temperatures. Only with use of microscopic properties that are sensitive to the small J_{inter} and at low enough temperatures is the 3D magnetic topology observed (as in muon-spin relaxation experiments).

The impact of the presence of odd- and even-membered finite chains in the crystals has also been evaluated. In the $CuPz(NO_3)_2$ crystal, odd-membered weakly interacting chains produce an increase in both $\chi(T)$ and $C_p(T)$ curves when the temperature is very close to zero, in good agreement with the experimental observations,[10,29] while even-membered chains produce a shoulder in the $C_p(T)$ curve between 0.8 and 5 K. No changes are seen in the remaining regions. Concerning the spin gap, odd-membered chains present a negligible spin gap but the finite even-membered chains still have a sizable one.

The spin gap for an open or cyclic infinite chain should be zero; however, it was estimated to be 0.176 and 0.077 cm^{-1}, respectively, because of the fact that larger chain models are required. Alternatively, we have proven that a zero spin gap is obtained by introducing the coexistence of odd- and even-membered finite chains within the crystal.

Finally, the effect of increasing the size of J_{inter} by 5 and 10 times was investigated by fixing the value of J_{intra} to that found in the 2 K $CuPz(NO_3)_2$ crystal. The magnetic susceptibility and heat capacity curves remain practically unchanged when using 3D models consisting of short-length chains.

Acknowledgment. The team from Universitat de Barcelona is thankful for support of the Spanish "Ministerio de Educación y Ciencia" (Grant CTQ2005-02329/UNBA05-33-001), the Catalan CIRIT (Grant 2005-SGR-00036/2005 PEIR 0051/69), and the CESCA and BSC−CNS for allocation of CPU time in their computers. M.D. thanks the Spanish Science and Education Ministry for the award of a "Ramón y Cajal" Fellowship. We thank S. Kimber for support with the neutron diffraction experiment. The U.S. team is grateful for grants from the NSF (Grant IMR-0314773) and the Kresge Foundation toward the purchase of the MPMS SQUID magnetometer.

Supporting Information Available: A CIF file for the 2 K crystal structure, complete ref 20, view of the 4s minimal magnetic model space employed to represent isolated chains (a 1D model) and the 4 × 2s and 4 × 4s models, both employed in representing interacting chains (that is, 3D models) (Figure S1), computed $\chi T(T)$ curve for the $CuPz(NO_3)_2$ crystal using the following 1D magnetic model spaces: 4s−12s [the experimental curve (●) obtained from powder samples is also shown] (Figure S2), computed heat capacity, $C_p(T)$, curve for the $CuPz(NO_3)_2$ crystal studied with crystallographic data determined at 2 K using the 12s−16s 1D cyclic magnetic model spaces with $J(d2) = -5.96$ cm^{-1} (Figure S3), energy spectrum of the 12 870 states corresponding to a 16s magnetic model space grouped according to the spin quantum number S of the state (Figure S4), (a) magnetic susceptibility curves and (b) heat capacity curves computed for the 2 × 7s and 2 × 8s models using different contributions of odd- and even-membered chains to the total macroscopic property (Figure S5). This material is available free of charge via the Internet at http://pubs.acs.org.